A Molecular Dynamics Study of the Structure of an $LiCl \cdot 4H_2O$ Solution

Philippe Bopp
Institut für Physikalische Chemie, Technische Hochschule Darmstadt, D-6100 Darmstadt

Isao Okada and Hitoshi Ohtaki
Department of Electronic Chemistry, Tokyo Institute of Technology at Nagatsuta, Yokohama, 227, Japan

Karl Heinzinger
Max-Planck-Institut für Chemie (Otto-Hahn-Institut), D-6500 Mainz,

Z. Naturforsch. **40 a**, 116–125 (1985); received December 10, 1984

Dedicated to Professor Dr. Alarich Weiss on the Occasion of his 60th Birthday

A study of the structure of a 13.9 molal aqueous LiCl solution has been performed by MD simulation. An improved central force model was used for water. The ion-water interactions were derived from ab initio calculations, while the ion-ion interactions were described by charged Lennard-Jones spheres. The structure function obtained from the simulation agrees reasonably well with that of X-ray diffraction. The number of first neighbour water molecules around an Li^+ is estimated to be about 5, as compared with a coordination number of about 4 derived from X-ray measurements. A small amount of contact ion pairs is suggested to exist. The O–H distance is increased by about 0.014 Å relative to pure water, resulting in a red shift of the O–H stretching frequency of about 300 cm^{-1}.

I. Introduction

It is interesting to explore how ions are solvated by water molecules in highly concentrated electrolyte solutions and how contact ion pairs are formed. However, this kind of study is scarce in the field of computer simulations as well as in experiments. In this study a 13.9 molal LiCl solution ($LiCl \cdot 4H_2O$) has been chosen. Although X-ray and neutron diffraction measurements have been performed for this solution [1], it is difficult to obtain information on the three dimensional structure from such data alone. This solution was studied formerly also by Molecular Dynamics (MD) simulation with the main purpose of analyzing X-ray diffraction data [2]. Empirically adjusted ion-ion potentials had been used in this study, while in the present work a combination of already known and tested potentials has been employed.

Reprint requests to Dr. K. Heinzinger, Max-Planck-Institut für Chemie, Saarstraße 23, P.O. Box 3060, D-6500 Mainz.

II. Potentials and Simulation Method

A modified version of the central force potential [3] has been employed, which had been used before in several simulations of pure liquid water [4, 5] and aqueous solutions [6–8]. It is very similar to the original central force potential in the latest version [9] as far as the intermolecular interactions are concerned, while the description of the intramolecular interactions has been improved significantly.

The ion-water pair potentials were based on those derived from ab initio calculations by Clementi et al. [10, 11]. As the central force potential [9] was used for water-water interaction, the parameters of the coulombic terms in the ion-water potentials were determined by the partial charges on the H and O atoms, 0.32983 e and 2×0.32983 e, respectively, and the ionic charge. These terms have then been subtracted from the potentials by Clementi et al. and the differences were fitted to simple analytical functions of the ion-oxygen and ion-hydrogen distances.

The resulting Li^+-water and Li^+-oxygen pair potentials are compared in Figure 1 with those given by Clementi and Popkie [10], and by Bounds and

0340-4811 / 85 / 0200-0116 $ 01.30/0. – Please order a reprint rather than making your own copy.

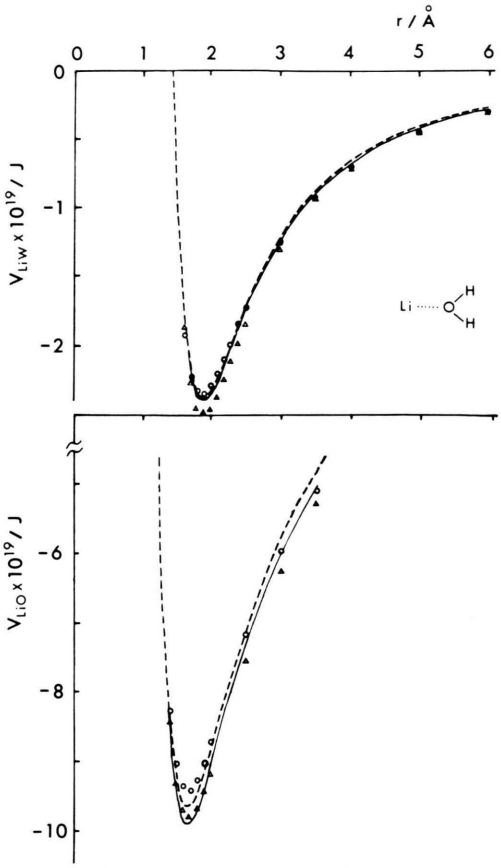

Fig. 1. Li^+-water (above) and Li^+-oxygen (below) pair potentials as a function of ion oxygen distance, for the water molecule orientation shown in the insertion. ——: the present potential; ---: its shifted force potential; ○: [10]; △: [12].

Table 1. Intermolecular potentials employed in the simulation. Energies are given in 10^{-19} J and the distances in Å. For intramolecular potentials see [3].

$$V_{OO}(r) = 10.04 + 1858/r^{8.86} - 0.01736\{\exp[-4(r-3.4)^2] + \exp[-1.5(r-4.5)^2]\}$$

$$V_{OH}(r) = -5.019/r + 0.433/r^{9.2} - 0.694/\{1+\exp[40(r-1.05)]\} - 0.278/\{1+\exp[5.493(r-2.2)]\}$$

$$V_{HH}(r) = 2.509/r + 6.94725/\{1+\exp[29.9(r-1.968)]\}$$

$$V_{LiO}(r) = -15.22/r + 1499\exp(-3.93r) - 8.109/r^2$$

$$V_{LiH}(r) = 7.609/r + 191\exp(-5.87r) + 3.934/r^2$$

$$V_{ClO}(r) = 15.22/r + 6304\exp(-3.21r) - 1.849/r^2$$

$$V_{ClH}(r) = -7.609/r + 3.138\times10^{24}\exp(-34.0r)$$

$$V_{LiLi}(r) = 23.07/r + 0.992\times10^{-2}[(2.37/r)^{12} - (2.37/r)^6]$$

$$V_{LiCl}(r) = -23.07/r + 0.512\times10^{-2}[(3.83/r)^{12} - (3.83/r)^6]$$

$$V_{ClCl}(r) = 23.07/r + 1.116\times10^{-2}[(4.86/r)^{12} - (4.86/r)^6]$$

Bounds [12], which have been calculated also from the original data of Clementi and Popkie by employing energy derivatives. There is no significant difference between these potentials. The pair potentials between Cl^- and water were those used in the simulation of an $MgCl_2$ solution [13], which were calculated also from the ab initio calculation [11] on the basis of the above stated procedure.

The ion-ion pair potentials were based on the model of a Lennard-Jones sphere with a unit elementary charge in the centre [14]. Although the pair potential for $Cl^- - Cl^-$ has been obtained also from ab initio calculations [13], the potential based on the Lennard-Jones model was adopted here for consistency with the oher ion-ion potentials. The difference between these two $Cl^- - Cl^-$ potentials is, in practice, very small, because at distances relevant in the simulation the coulombic repulsion is the main term in both cases.

The pair potentials thus obtained are given in Table 1.

The "shifted force potential" method [15, 16] was applied to ensure a constant-energy run. The Li^+-water and Li^+-oxygen pair potentials modified in this way are also shown in Figure 1. The Ewald method was used for the calculation of the coulombic interactions. A predictor-corrector algorithm [17] was employed. The number of H, O, Li^+ and Cl^- in the periodic cube was 288, 144, 36 and 36, respectively, with an edge length $L = 17.732$ Å calculated from the measured density (1.2272 g cm^{-3} [18]). The time step was 2.5×10^{-16} s. The simulation extended over 3600 time steps after equilibration, the initial configuration being taken from the former MD simulation [2]. The average temperature was 314 K.

III. Results and Discussion

A) Radial distribution function (RDF)

X-ray and neutron weighted structure functions are obtained from the partial radial distribution functions $g_{ij}(r)$ by

$$k \cdot i(k)_{X,N} = \frac{\sum_i \sum_j x_i x_j \xi_i \xi_j}{(\sum_i x_i \xi_i)^2} \cdot \int_0^l 4\pi\varrho r (g_{ij}(r) - 1)\sin(kr)\,dr, \quad (1)$$

where k is the scattering vector, that is $k = 4\pi\sin\theta/\lambda$ (2θ: scattering angle, λ: wavelength of incident

radiation); ξ denotes the atomic scattering factor $f(k)$ for X-ray functions $i(k)_X$ and the scattering length b for neutron functions $i(k)_N$; x is the mole fraction and ϱ is the number density defined here as the number of molecules of ($LiCl + H_2O$) per $Å^3$, that is 0.0323 $Å^{-3}$; l is an upper limit of distance for integrations and taken here to be $L/2$.

The structure function obtained from the MD is compared with that from X-ray diffraction [2] in Figure 2. Satisfactory agreement is obtained between them, although some discrepancies are found at a higher k region ($> 12\,Å^{-1}$) where the X-ray diffraction data might contain relatively large uncertainties due to low scattered intensities. This agreement suggests that the intermolecular configurations obtained by the present simulation sufficiently reproduces the real system.

The total X-ray weighted RDF $G(r)_X$ is calculated from the structure function by

$$G(r)_X = 1 + \frac{1}{2\pi^2 \varrho r} \cdot \int_0^{k_{max}} k \cdot i(k)_X M(k) \sin(k r)\, dk\,, \qquad (2)$$

where k_{max} is taken as $15\,Å^{-1}$ and $M(k)$ is a modification function which is put as $M(k) = \exp(-0.01\,k^2)$ in order to eliminate the truncation error of the Fourier transform and to minimize the uncertainty of the $k \cdot i(k)_X$ value at higher k values. The X-ray weighted radial distribution functions $G(r)_X$ obtained from the MD simulation and the experiment are compared in Figure 3. The agreement between the calculated and experimentally obtained radial distribution curves is, in general, satisfactory, although a difference is found at a peak around 2 Å, where mainly interactions between Li^+ and water molecules contribute (see below).

In Figure 4 the neutron structure function $k \cdot i(k)_N$ calculated by Eq. (1) is compared with the experimental one [19]. As the scattering length of O, D, Li and Cl atoms, the values of $b = 0.5805$, 0.6674, -0.190 and 0.95792×10^{-12} cm [20] are adopted, respectively. The contribution only from the O–H and H–H pairs as derived from the MD result, is shown as dotted line. This indicates that in the case of the $k \cdot i(k)_N$ the contribution is due mainly to the O–H(D) and H(D)–H(D) pairs and wholly so above $9\,Å^{-1}$. As the agreement of the phases at a high k region between the MD and experimental

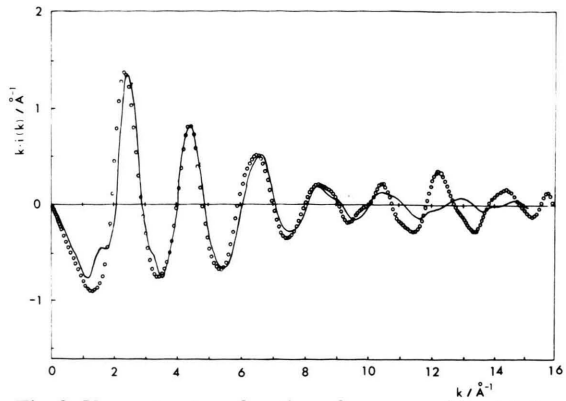

Fig. 2. X-ray structure functions from experiment (○) and MD simulation (——).

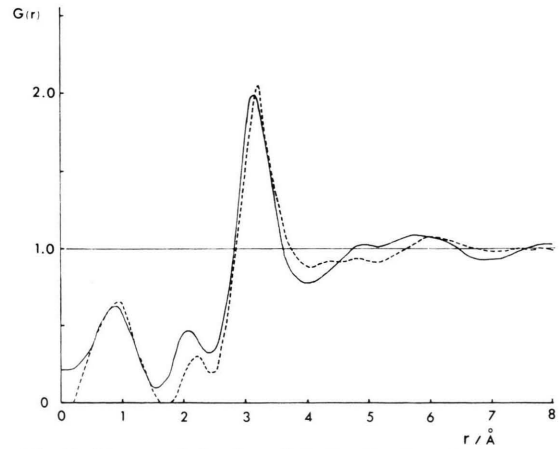

Fig. 3. X-ray weighted radial distribution functions from experiment (- - -) and MD simulation (——).

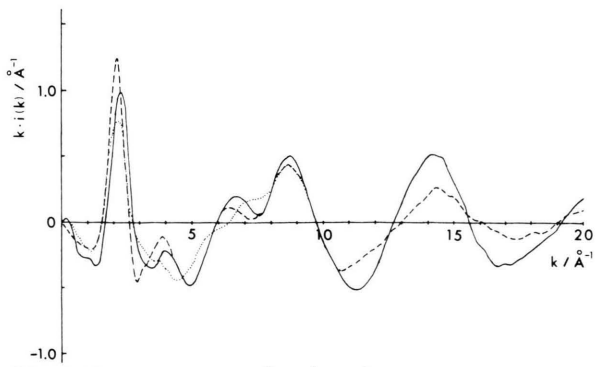

Fig. 4. Neutron structure functions from experiment (- - -), MD simulation (——), and the O–H and H–H pair contributions of the latter only (· · · · ·).

Table 2. Characteristic values for the radial distribution functions $g_{ij}(r)$. The distances are given in Å with an uncertainty of at least ± 0.02 Å. r_{M1}, r_{m1}, and r_{M2} are the distances at the first maximum, the first minimum, and the second maximum, respectively. R_1 and R_2 are the distances where $g_{ij}(r)$ crosses unity for the first and the second time, respectively. For O–H and H–H only intermolecular data are given. The uncertainty in $g_{ij}(r)$ can be estimated from Figures 5–8. n is the coordination number as defined in the text.

i	j	R_1	r_{M1}	$g(r_{M1})$	R_2	r_{m1}	$g(r_{m1})$	r_{M2}	$g(r_{M2})$	$n(R_2)$	$n(r_{m1})$
Li	O	1.81	2.00	9.98	2.50	3.02	0.23	4.28	1.05	4.7	5.2
Li	H	2.43	2.70	4.65	3.08	3.35	0.45	4.88	1.15	9.6	10.7
Cl	O	2.89	3.20	3.66	3.69	4.10	0.71	5.60	1.31	6.5	8.2
Cl	H	1.92	2.25	3.03	2.63	2.92	0.64	3.45	1.41	5.2	6.3
Li	Li	2.8	3.0	2.9	3.6	4.4	0.2	6.1	1.0	1.4	1.8
Li	Cl	3.9	2.8	0.5	5.4	3.2	0.1	4.8	2.9	6.0	0.1
Cl	Cl	4.4	4.9	2.2	5.7	6.4	0.7	8.3	1.3	4.4	6.3
O	O	2.69	2.98	2.91	3.54	3.93	0.69	5.90	1.14	5.4	6.8
O	H	2.84	2.00	0.24	4.21	2.28	0.20	3.20[a] 3.78	1.35 1.43	17.6	2.3
H	H	2.20	2.25	1.11	2.35	2.73	0.82	3.65	1.24	1.7	3.2

[a] The second peak is splitted into two peaks.

results is rather good, the intramolecular structure of the water molecule is inferred to be well simulated.

The characteristic values of the radial distribution functions $g_{ij}(r)$ for the 10 pairs are given in Table 2.

In Figure 5 $g_{LiO}(r)$ and $g_{LiH}(r)$ are shown. The maximum of the first – very sharp – peak in $g_{LiO}(r)$ is positioned at 2.00 Å. Data on first neighbour Li^+-water distances are significantly different in X-ray and neutron diffraction, the reason for which remains to be known. With one exception (see [1]) the neutron data [19, 21–23]) lead to Li^+-O distances between 1.90–2.00 Å, while most of the X-ray data are above 2.10 Å (see Tables in [2, 24]). Thus, the present result is closer to that obtained by neutron diffraction, while simulations at lower concentrations with the ST2 and MCY models for water [25, 26] lead to Li^+-O distances in agreement with X-ray data. In this highly concentrated solution, g_{LiO} does not become zero at the first minimum position r_{m1}, which is in contrast with the results obtained in dilute solutions.

When the position of the first maximum, r_{M1}, in g_{LiH} is compared with neutron diffraction results at comparable concentrations, it agrees well with that determined by Narten et al. (2.68 ± 0.01 Å at $LiCl \cdot 4.01\,H_2O$ [1]) but is appreciably greater than that obtained with the first-order difference method by Newsome et al. (2.50 ± 0.02 Å at a 9.95 molal LiCl solution [21]).

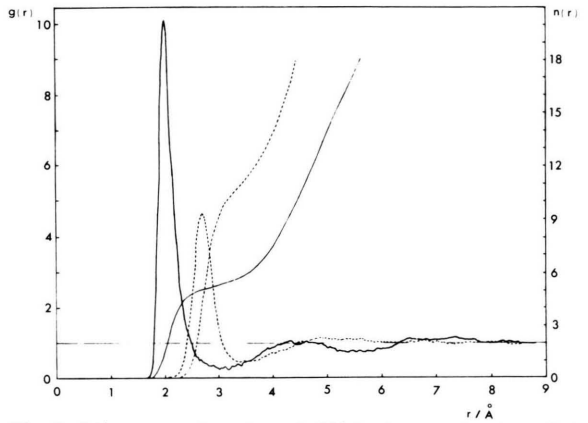

Fig. 5. Li^+-oxygen (——) and Li^+-hydrogen (- - -) radial distribution functions and running integration numbers.

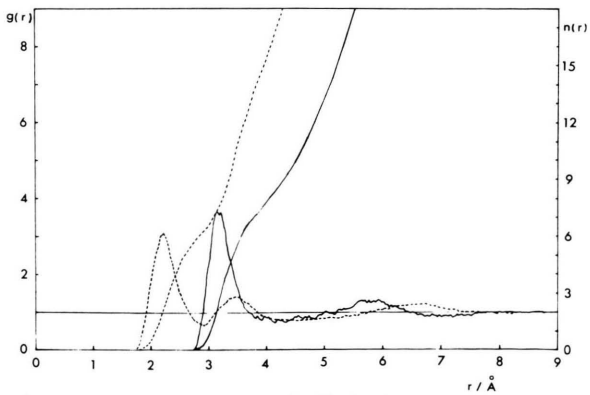

Fig. 6. Cl^--oxygen (——) and Cl^--hydrogen (- - -) radial distribution functions and running integration numbers.

It can be seen from Fig. 6 and Table 2 that the Cl^--water first neighbour distance of 3.20 Å is in excellent agreement with the value determined so far by X-ray diffraction [1, 2, 27]. Since the contribution of the Cl–O pair to $i(k)$ and $G(r)$ is dominant in X-ray measurements of aqueous LiCl solutions particularly at this high concentration, the Cl–O distance can be measured very accurately. Therefore, this agreement between the MD simulation and the experiment indicates that the configuration simulated here reproduces the real system well. A neutron diffraction experiment at a comparable concentration ($LiCl \cdot 5.58 H_2O$) yielded a Cl–O distance of 3.29 ± 0.04 Å [28].

The two peaks in $g_{ClH}(r)$ (H atoms within the same water molecule) are separated distinctively, consistent with the formation of linear hydrogen bonds between the water molecules and Cl^-, as discussed in detail below. r_{M1} and r_{M2} in $g_{ClH}(r)$ (see Table 2) are in good agreement with the results of the neutron diffraction (2.22 ± 0.02 Å and 3.50 – 3.68 Å, respectively, in $LiCl \cdot 5.58 H_2O$ [28]).

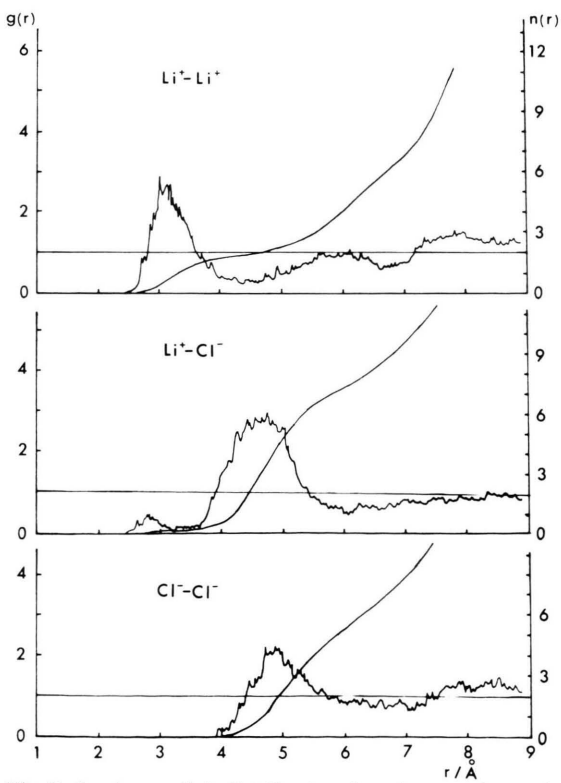

Fig. 7. Ion-ion radial distribution functions and running integration numbers.

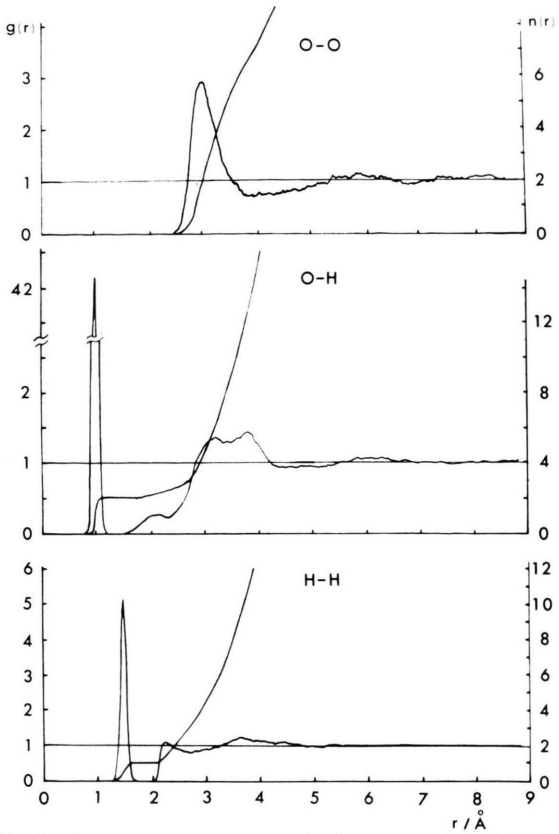

Fig. 8. Oxygen-oxygen, oxygen-hydrogen, and hydrogen-hydrogen radial distribution functions and running integration numbers.

The ion-ion RDFs are shown in Fig. 7 along with the running integration numbers. It is hard to determine the peak positions of these ion pairs by X-ray diffraction. The first-order and the second-order difference method by neutron diffraction [29] may be applicable for this purpose [23].

The position of the first peak in $g_{LiLi}(r)$ appears at a distance shorter by as much as 2 Å than in a 2.2 molal LiI solution [30]. This peak results from a configuration where two Li^+ ions are coordinated by the same water molecule.

The $g_{LiCl}(r)$ curve (Fig. 7) showing a small peak at about 2.8 Å indicates the formation of contact ion pairs. The amount of ion pairing is so small that its existene cannot be ascertained experimentally. The second big and wide peak in $g_{LiCl}(r)$ around 4.5 Å is due to two ions separated by one water molecule. The broad peak shows that the distribution of the dipole directions around Li^+ and Cl^- is widely spread, as will be shown below. The running in-

tegration number is 6 to 7 within the second minimum position, r_{m2}, and nearly equal to that of the water molecules around a Cl^-. This is also consistent with the high probability for Li^+-Cl^- pairs separated by one water molecule.

The peak in $g_{ClCl}(r)$ around 4.9 Å results mainly from two Cl^- linked by two hydrogen atoms within a water molecule.

The $g_{OO}(r)$, $g_{OH}(r)$, and $g_{HH}(r)$ functions are shown in Figure 8.

The $g_{OO}(r)$ curve has a first maximum at 2.98 Å, a distance slightly larger than that in pure water simulated by using the same pair potentials (2.85 Å [4]). The peak height is almost the same in both cases. The coordination number is 6.8 within r_{m1} (Table 2). Such a coordination number may result, for example, from a typical case: when a water molecule of the octahedral hydration shell of an Li^+ belongs at the same time to the hexahedral one of a Cl^-, this water molecule has a water-coordination number of 7 (4 from the former and 3 from the latter). The second peak of $g_{OO}(r)$ is much less pronounced than in pure water. This may be due to breakage in the hydrogen-bond network of the water structure.

The main characteristic of $g_{OH}(r)$ as compared to that in pure water and in dilute solutions is the very low peak height at ca. 2.0 Å and an appearance of a peak at ca. 3.8 Å. This result, together with the running integration number which shows only a slight increase around 2 Å, indicates that hydrogen bonding between water molecules is rare. Only ca. 0.3 hydrogen atoms of neighbouring water molecules are located within the distance of a normal hydrogen bond. This is in keeping with the distribution of the potential energies between pairs of water molecules (see below). The peak around 3.8 Å may result from two water molecules coordinated to the same Li^+ where the rotational motions around the dipole moments are considerably hindered.

Additional support for a low probability for the existence of normal hydrogen bonding comes from the peak height of $g_{HH}(r)$ at ca. 2.3 Å, which is significantly smaller than that in pure water and dilute solutions.

B) Hydration shell properties

The curve of the running integration number in Fig. 5 shows that n_{LiO} is about 4.7 at R_2 (= 2.50 Å) and 5.2 at r_{m1} (= 3.02 Å). Thus, even in such a highly concentrated solution where the molar ratio of water molecules to an Li^+ is 4, the coordination number is more than 4. This means that about half of the water molecules coordinate to more than one Li^+ at the same time.

The running integration number n_{ClH} is about 5.2 at R_2 (= 2.63 Å) and 6.3 at r_{m1} (= 2.92 Å). The $n_{ClO}(r)$ has almost the same value ($\cong 6.5$) at R_2 (= 3.69 Å).

The distributions of coordination numbers of oxygen atoms around an Li^+ and a Cl^- within R_2 and r_{m1} are given in Figure 9. The distribution is peaked at 6 for an Li^+ and 8 for a Cl^-, when r_{m1} is defined as the limit of the coordination sphere.

The angular distribution function of the coordinating water molecules around the ions within r_{m1} is calculated by

$$P(\psi) = C\, n(\psi)/\sin\psi\,, \tag{3}$$

where $n(\psi)$ is the number of pairs of water molecules at an angle ψ centred on an ion; C is a normalization factor chosen so that $\int_0^{180} P(\psi)\, d\psi = 1$.

Figure 10 shows that there are two peaks at 88° and 180°, which indicates that water molecules are nearly regular-octahedrally located around an Li^+.

In the case of water molecules around a Cl^- (see Fig. 11), there is a peak at 51°. This angle corresponds to an angle produced by two water molecules in the first hydration shell of Cl^- and separated from each other by nearly a normal distance between neighbouring water molecules in pure water.

C) Orientation of the water molecules

The average dipole moment direction of water molecules $\langle\cos\theta\rangle$ is expressed as a function of distance from the ions in Fig. 12, where θ is the angle between the dipole moment direction and the vector pointing from the oxygen atom toward the ion.

For Li^+ the $\langle\cos\theta\rangle$ value is -0.93 ($\theta = 158°$) at the smallest Li^+-O distance in g_{LiO} and increases rather sharply in the region up to 6 Å. This is in contrast to the case of dilute solutions. In a 2.2 molal LiI solution $\langle\cos\theta\rangle$ is nearly constant over the range 2 to 3 Å [30]. The remarkable change in $\langle\cos\theta\rangle$ with distance in the present case is obviously due to the very high concentration of the ions in the solution in which a water molecule coordinates to more than one ion and therefore its orientation is necessarily affected by both ions at the same time.

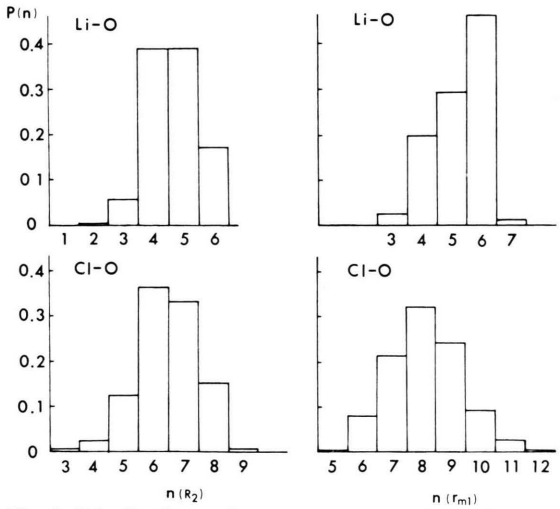

Fig. 9. Distributions of coordination numbers of oxygen atoms around Li^+ and Cl^-. The coordination spheres are taken within R_2 (left) and r_{m1} (right).

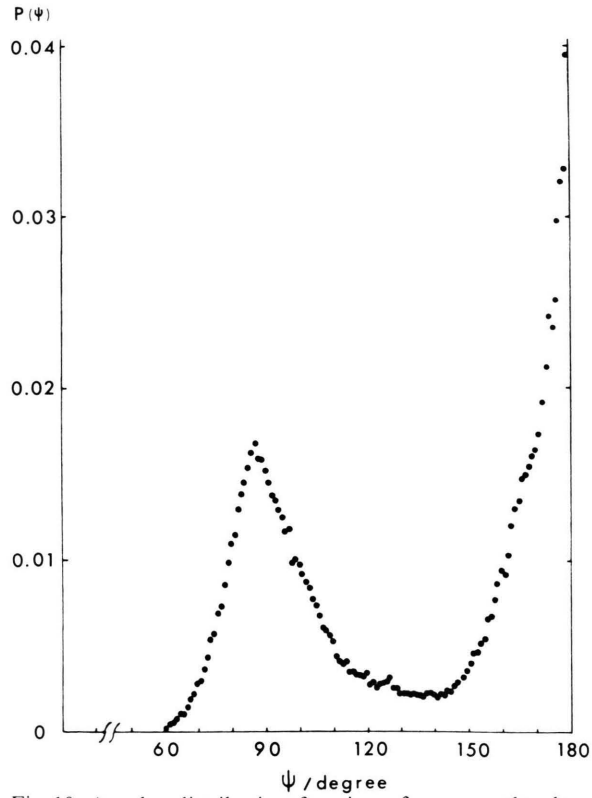

Fig. 10. Angular distribution function of water molecules within r_{m1} around an Li^+.

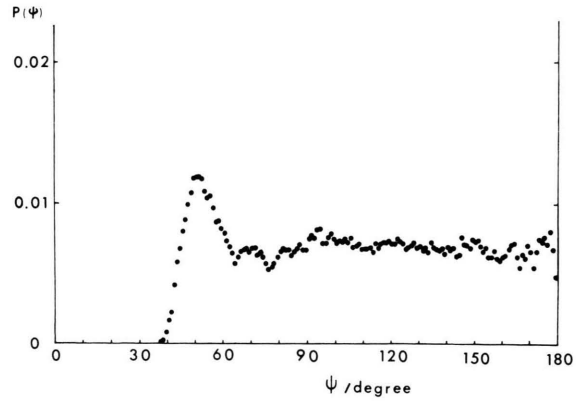

Fig. 11. Angular distribution function of water molecules within r_{m1} around a Cl^-.

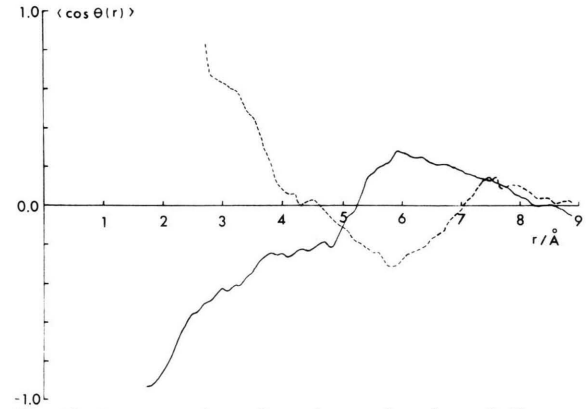

Fig. 12. Average value of $\cos\theta$ as a function of distance from Li^+ (——) and Cl^- (- - -). θ is defined in the text.

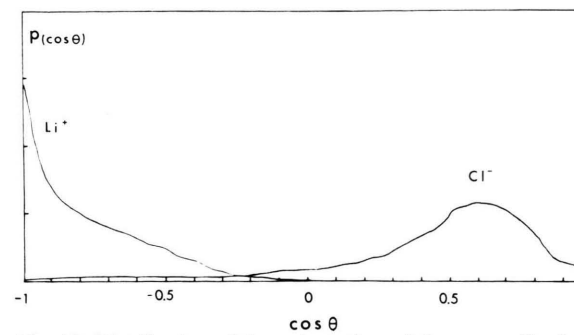

Fig. 13. Distribution of the orientation of the water dipoles in the first hydration shells of Li^+ and Cl^-. θ is defined in the text.

For Cl^- $\langle \cos\theta \rangle$ is about 0.81 ($\theta = 36°$) at the smallest $Cl^- - O$ distance and very sharply decreases to 0.68 ($\theta = 47°$). This suggests that the number of water molecules forming linear hydrogen bonds with the ion is small, which is due to the influence of the neighbouring ions, as stated above.

The distribution of $\cos\theta$ is given in Fig. 13 for molecules within r_{m1} around Li^+ and Cl^-. The values of θ are broadly distributed.

In the hydration shell of Li^+ within r_{m1} (= 3.02 Å) a distribution is found with a maximum of $\cos\theta = -1.0$ and an average value of -0.76 corresponding to $\theta = 139°$. This is similar to the case of water molecules around Na^+ in a 2.2 molal NaCl solution (average value of $\theta = 140°$) [6, 31], although this agreement may be fortuitous.

For the water molecules around Cl^- within r_{m1} (= 4.10 Å) a maximum is found at $\cos\theta = 0.60$ ($\theta = 53°$) and an average value at 0.45 ($\theta = 63°$), while for a certain fraction of the water molecules $\cos\theta$ is even negative. The distribution of $\cos\theta$ over a wide range has also been found in dilute solutions [13], although this trend is more pronounced here.

D) Average potential energy and pair interaction energy distribution

The average potential energy of water molecules (W) around Li^+ and Cl^- is shown in Fig. 14 as a function of ion-oxygen distance. The $\langle V_{LiW}(r) \rangle$ curve increases with distance in the range from 1.9 to 6.0 Å. No maximum is found in $\langle V_{LiW}(r) \rangle$ around the position of the first minimum in g_{LiW}, which is in contrast to the case for 2.2 molal alkali halide solutions [30]. In the region above 5.4 Å $\langle V_{LiW}(r) \rangle$ becomes positive. This is because the water molecules in this region are affected more strongly by other neighbouring ions than by the Li^+ at the reference position.

The positions of the first maxima in the corresponding RDFs, which are marked by arrows in Fig. 14, are found at slightly greater distances both for Li^+ and Cl^- than at the potential minima. In dilute solutions such as a 1.1 molal aqueous $MgCl_2$ solution [13], the minimum of the average potential energy and the position of r_{M1} for Cl^--water pairs coincide at 3.2 Å. In the present case the position of the potential minimum is located at about 3.0 Å.

The average potential energy $\langle V_{WW}(r) \rangle$ for water-water pairs has positive values in the range up to about 7 Å (Figure 15). This is not observed in dilute solutions. In highly concentrated solutions such as the present one the ions force the water molecules into orientations relative to each other which are very unfavourable from an energetic point of view. A particularly large positive value at the region where two water molecules are closely neighboured indicates that water molecules coordinating to the same Li^+ are unfavourably orientated with respect to each other from an energetic standpoint.

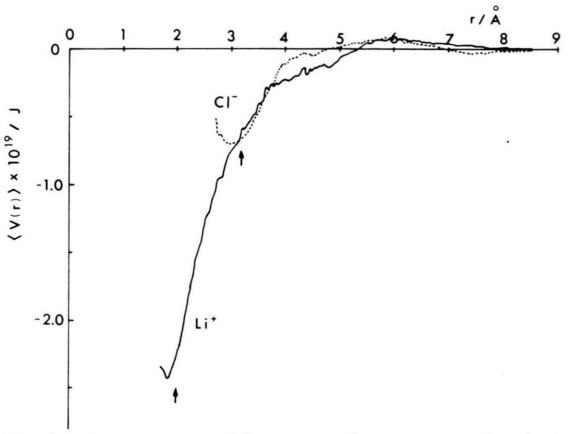

Fig. 14. Average potential energy of a water molecule in the field of the Li^+ (——) and the Cl^- (·····) as a function of ion-oxygen distance.

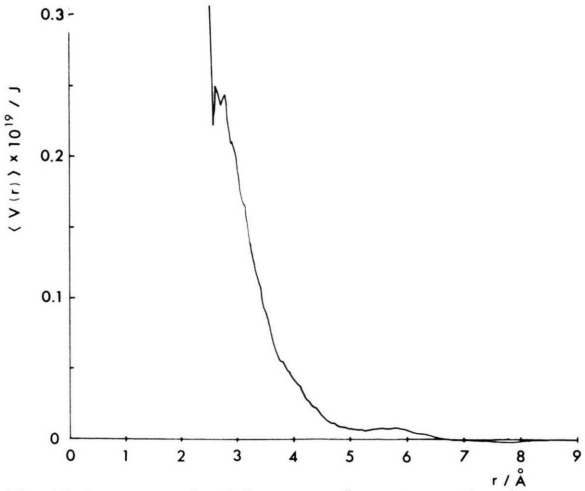

Fig. 15. Average potential energy of a water molecule as a function of oxygen-oxygen distance.

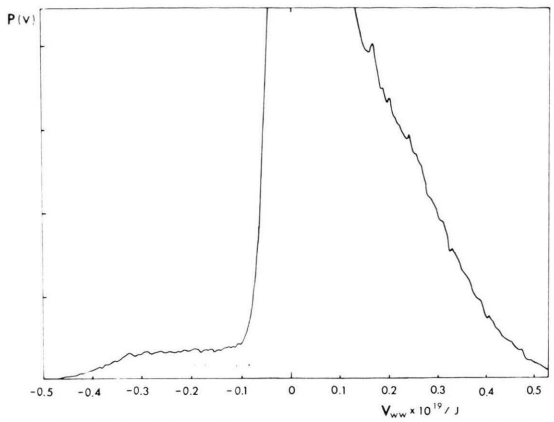

Fig. 16. Pair interaction energy distribution $P(V)$ for water-water. $P(V)$ is given in an arbitrary unit.

The energetically unfavourable orientation of water molecule pairs can be also inferred from the potential energy distribution in Figure16. A relatively large distribution in the positive energy region up to 0.6×10^{-19} J is found. In the negative region of $\langle V_{WW}(r) \rangle$ the distribution is small and no maximum is found, which indicates that a very small portion of water molecule pairs is linked by normal hydrogen bonds.

E) Intramolecular configuration of the water molecule

Since the water molecule is deformable under the potential field used in this study, the deformation by the effect of surrounding particles can be observed. The g_{OH} curve has a sharp maximum at 0.985 Å, while the average O−H length is 0.9899 Å, which is larger than 0.9755 Å in pure water using the same model [7]. The average angle H−O−H is 97.25°, which is smaller than 100.9 to 101.4 found in pure water [3]. The average dipole moment is 6.90×10^{-30} C m (2.07 D).

The frequency due to OH stretching vibration appears at 3210 cm^{-1}, which is calculated by Fourier transformation from the velocity autocorrelation function. This value is 300 cm^{-1} lower than that of the pure water (3510 cm^{-1} [3]). As the O−H stretching frequency is known to decrease by $\cong 20000$ cm^{-1}/Å with increasing O−H distance [32], the increase of 0.0144 Å from 0.9755 Å to 0.9899 Å corresponds to a red shift of 290 cm^{-1}. Thus, the shift of 300 cm^{-1} indicates an internal consistency of the water potential used here. This large shift is also qualitatively consistent with that found for hydration water molecules of Ca^{2+} in the MD simulation of a 1.1 molal $CaCl_2$ solution using the same water model [7]. However, the result of an infrared study of a saturated LiCl solution shows a 5 cm^{-1} blue shift for the O−H frequency [33]. Another infrared study of concentrated LiCl solutions under high pressure also suggests a small blue shift [34]. This discrepancy in the results between the simulation and the experiments cannot be resolved at the moment.

Acknowledgement

This work has been done under an international collaboration program sponsored by Deutsche Forschungsgemeinschaft and Japan Society for Promotion of Sciences. For a part of the calculations the HITAC 200-H computers at the Institute for Molecular Science at Okazaki and National Laboratory for High Energy Physics at Tsukuba were used. The other part of the calculations was performed on the Cray I at the computer centre of the Max-Planck-Institut für Plasmaphysik in Garching.

[1] A. H. Narten, F. Vaslow, and H. A. Levy, J. Chem. Phys. **58,** 5017 (1973).
[2] I. Okada, Y. Kitsuno, H.-G. Lee, and H. Ohtaki, in: Ions and Molecules in Solution (N. Tanaka, H. Ohtaki, and R. Tamamushi, eds.), Elsevier, Amsterdam 1983, p. 81.
[3] P. Bopp, G. Jancsó, and K. Heinzinger, Chem. Phys. Lett. **98,** 129 (1983).
[4] G. Jancsó, P. Bopp, and K. Heinzinger, Chem. Phys. **85,** 377 (1984).
[5] G. Pálinkás, P. Bopp, G. Jancsó, and K. Heinzinger, Z. Naturforsch. **39a,** 179 (1984).
[6] G. Jancsó, K. Heinzinger, and T. Radnai, Chem. Phys. Lett. **110,** 196 (1984).
[7] M. M. Probst, P. Bopp, K. Heinzinger, and B. M. Rode, Chem. Phys. Lett. **106,** 317 (1984).
[8] M. M. Probst, T. Radnai, K. Heinzinger, P. Bopp, and B. M. Rode, J. Phys. Chem., in press.
[9] F. H. Stillinger and A. Rahman, J. Chem. Phys. **68,** 666 (1978).
[10] E. Clementi and H. Popkie, J. Chem. Phys. **57,** 1077 (1972).
[11] H. Kistenmacher, H. Popkie, and E. Clementi, J. Chem. Phys. **58,** 5627 (1973).
[12] D. G. Bounds and P. J. Bounds, Mol. Phys. **50,** 25 (1983).
[13] W. Dietz, W. O. Riede, and K. Heinzinger, Z. Naturforsch. **37a,** 1038 (1982).

[14] G. Pálinkás, W. O. Riede, and K. Heinzinger, Z. Naturforsch. **32a,** 1137 (1977).
[15] W. B. Streett, D. J. Tildesly, and G. Saville, ACS Symposium Series **86,** 144 (1978).
[16] Gy. I. Szász and K. Heinzinger, Z. Naturforsch. **34a,** 840 (1979).
[17] K. Heinzinger, W. O. Riede, L. Schäfer, and Gy. I. Szász, ACS Symposium Series **86,** 1 (1978).
[18] E. W. Washbuhn (Ed.), International Critical Tables of Numerical Data Physics, Chemistry and Technology, **Vol. III,** Maple Press, York 1928, p. 77.
[19] Y. Tamura, T. Yamaguchi, I. Okada, H. Ohtaki, M. Misawa, and N. Watanabe, unpublished.
[20] V. F. Sears, AECL-8490, Chalk River, Ontario 1984.
[21] J. R. Newsome, G. W. Neilson, and J. E. Enderby, J. Phys. C: Solid State Phys. **13,** L923 (1980).
[22] N. Ohtomo and K. Arakawa, Bull. Chem. Soc., Japan **52,** 2755 (1979).
[23] K. Ichikawa, T. Kameda, T. Matsumoto, and M. Misawa, J. Phys. C: Solid State Phys. **17,** L725 (1984).
[24] Gy. I. Szász, K. Heinzinger, and G. Pálinkás, Chem. Phys. Lett. **78,** 194 (1981).
[25] T. Radnai, G. Pálinkás, Gy. I. Szász, and K. Heinzinger, Z. Naturforsch. **36a,** 1076 (1981).
[26] M. Mezei and D. L. Beveridge, J. Chem. Phys. **74,** 6902 (1981).
[27] R. M. Lawrence and R. F. Kruh, J. Chem. Phys. **47,** 4758 (1967).
[28] S. Cummings, J. E. Enderby, G. W. Neilson, J. R. Newsome, R. A. Howe, W. S. Howells, and A. K. Soper, Nature, London **287,** 714 (1980).
[29] J. E. Enderby and G. W. Neilson, Adv. Phys. **29,** 323 (1980).
[30] Gy. I. Szász, K. Heinzinger, and W. O. Riede, Z. Naturforsch. **36a,** 1067 (1981).
[31] P. Bopp, W. Dietz, and K. Heinzinger, Z. Naturforsch. **34a,** 1424 (1979).
[32] S. I. Laplaca, W. C. Hamilton, B. Kamb, and A. Prakash, J. Chem. Phys. **58,** 567 (1973).
[33] R. D. Waldron, J. Chem. Phys. **26,** 809 (1957).
[34] V. M. Valyashko, M. Buback, and E. U. Franck, Z. Naturforsch. **35a,** 549 (1980).